Proceedings of IMECE'02
2002 ASME International Mechanical Engineering Congress and Exposition
New Orleans, Louisiana, November 17-22, 2002

IMECE2002-33309

DESIGN AND CHARACTERIZATION OF A MEMS PIEZORESISTIVE COCHLEAR-LIKE ACOUSTIC SENSOR

Robert D. White
Vibrations and Acoustics Laboratory
Department of Mechanical Engineering
University of Michigan
Ann Arbor, Michigan 48109
Email: rdwhite@umich.edu

Karl Grosh*
Vibrations and Acoustics Laboratory
Department of Mechanical Engineering
University of Michigan
Ann Arbor, Michigan 48109
Email: grosh@umich.edu

ABSTRACT

The mammalian cochlea achieves excellent acoustic transduction though the use of mechanical signal processing. The device presented in this paper mimics the structure of the cochlea with a micromachined array of nearly 3000 0.34 μm thick silicon beams suspended between two wafer-high ducts. Piezoresistive strain gauges are incorporated into the beams to produce 38 channels of realtime frequency information. Device mechanical and electrical models are presented. Initial mechanical measurements in air demonstrate good agreement with predicted frequency sensitive and response amplitude. Device sensitivity in air is tentatively measured to be 30 mm/s of beam center velocity response per Pascal of input pressure, corresponding to a predicted piezoresistor sensitivity of 7000 ppm/Pa. This gives an expected achievable resolution of 250 μPa_{rms} in a 100 kHz band in air. Note that this differs from the intended operating mode of the transducer, which is in fluid over a 20 kHz band.

INTRODUCTION

The mammalian cochlea, the inner part of the ear, functions as a realtime mechanical signal analyzer, separating incoming acoustic energy into frequency components for transmission to the brain. The mechanical structure provides a compact and robust mechanism for delivering approximately 3000 channels of frequency information. The human cochlea operates over a 3 decade band in frequency, 120 dB of dynamic range, and can distinguish tones which differ less than 0.5%. Partly due to these excellent transduction characteristics, its mechanics have been extensively studied, both mathematically and experimentally.

Physically, the cochlea consists of a series of curved, fluid-filled ducts separated by membranes. One of the cochlear membranes, the basilar membrane, has mechanical properties that vary gradually along the length of the duct, giving rise to a slowly varying acoustic impedance. Due to this varying impedance, an incoming acoustic wave induces amplified membrane motion at a specific location, dependent on the frequency of the excitation. The induced motion, through fluidic interaction, stimulates inner hair cells that send information to the brain. A simplified model of this structure has been extensively studied using Wentzel-Kramer-Brillouin (WKB) asymptotic techniques. Such cochlear modeling methods are appropriate for the fluid-loaded system where a traveling wave is produced. Modeling of the system response to normally incident plane waves in the absence of a traveling wave can be more accurately accomplished by considering the membrane as an array of uncoupled fluid-loaded beams. Such a model is more applicable for the experimental results shown in this paper. The cochlear model achieves a much sharper frequency cutoff than the beam oscillator array.

Microfabrication technology allows these cochlear-like structures to be mimicked at the size scale of the biological system. We present a design for a silicon cochlea that extends previous work by utilizing a micromachined liquid-filled two-duct structure and a beam array which captures the orthotropic properties of the basilar membrane in the biological cochlea. A micro-

*Address all correspondence to this author.

Copyright © 2002 by ASME

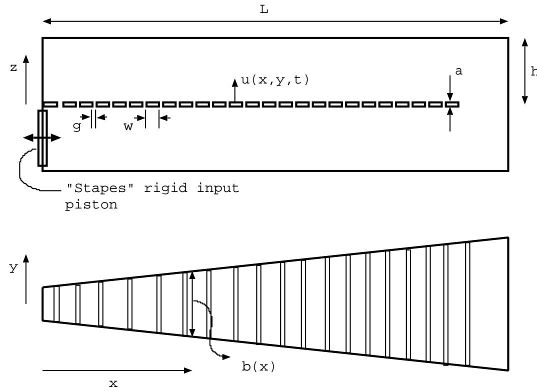

Figure 1. SCHEMATIC OF COCHLEAR TRANSDUCER GEOMETRY

fabrication process for producing such a structure has been developed and implemented. The active structure is a 3400 Å thick silicon membrane comprised of a series of parallel beams, whose length varies from 70 μm to 1.8 *mm*. These beams are suspended between two wafer-thick through-etched ducts. Transduction of mechanical motion to an electrical signal is accomplished using boron-doped silicon piezoresistive elements integrated into the mechanical structure. Modeling, design, fabrication, and experimental results for the structure will be discussed.

Modeling

The mechanical structure of the cochlear-like sensor consists of two fluid-filled rectangular cross-section ducts of constant height but varying width, separated by a closely-spaced array of parallel beams, as diagrammed in Figure 1. The functional dependence of the beam array width on longitudinal position, $b(x)$, produces a varying acoustic impedance with x, and gives rise to the acoustic localization phenomenon which we are attempting to produce. The beam width, w, is kept much larger than the beam gap, g, to keep the beam array as similar as possible to a continuous membrane. To achieve logarithmic frequency to linear position mapping, an exponential duct width function, $b = b_0 e^{\alpha \cdot x/L}$, is chosen.

Ten different device designs were fabricated on each wafer. All ducts are 3 *cm* long (L=3 *cm*) and wafer high (h=0.5 *mm*). Additional geometric parameters as given in Table 1.

Device	Designed Bandwidth	Gap Width	Beam Width	Membrane Profile
1: 4A-1	20 Hz - 20 kHz	2 μm	10 μm	70 - 1800 μm
2: 4A-2	20 Hz - 20 kHz	4 μm	15 μm	70 - 1800 μm
3: 4A-3	20 Hz - 20 kHz	3 μm	10 μm	70 - 1800 μm
4: 4A-4	20 Hz - 20 kHz	3 μm	20 μm	70 - 1800 μm
5: 4B-1	100 Hz - 5 kHz	2 μm	10 μm	140 - 1000 μm
6: 4B-2	100 Hz - 5 kHz	4 μm	15 μm	140 - 1000 μm
7: 4B-3	100 Hz - 5 kHz	3 μm	10 μm	140 - 1000 μm
8: 4B-4	100 Hz - 5 kHz	3 μm	20 μm	140 - 1000 μm
9: 4C-1	200 Hz - 10 kHz	3 μm	15 μm	100 - 800 μm
10: 4C-2	200 Hz - 10 kHz	2 μm	15 μm	100 - 800 μm

Table 1. DETAILS OF DESIGN GEOMETRY

Wentzel-Kramer-Brillouin Cochlear Modeling

The modeling problem can be broken into two domains. We assume an incompressible (acoustic wavelengths are much longer than structural dimensions), inviscid fluid in the bulk of the fluid domain, with a viscous layer providing damping close to the beam array. The structural layer is modeled as an orthotropic Kirchoff plate (Graff, 1975; J.T. Oden and E.A. Ripperger, 1981). In the case of a beam array, the orthotropy is taken to the limit, with zero longitudinal stiffness. ($E_x << E_y$) Coupling between the domains occurs via pressure loading of the structure, and a corresponding velocity boundary condition on the fluid domain.

A technique which has been applied to solve the equations arising from this system is the Wentzel-Kramer-Brilluoin (WKB) technique. This is a useful technique for solving systems with a slowly spatially varying parameter and an oscillatory solution, where the varying parameter is almost constant over one wavelength of the solution. In our case, the beam array width, $b(x)$, is the slowly varying parameter. We assume a solution for the beam array response with a slowly varying amplitude, $W(x)$, and phase, $\Theta(x)$. A single structural cross-mode, $\psi(y)$ is utilized to simplify computation. The displacement of the beam array is a function of x, y and t:

$$u(x,y,t) = W(x)e^{i\theta(x,t)}\psi(y) \quad \text{where} \quad \theta(x,t) = \int k_x(x)dx - \omega t \tag{1}$$

With this in hand, an expression can be derived for the energy in the system, which can be minimized to obtain solutions for the slowly varying amplitude and phase of the beam array response. Work by other authors (C. R. Steele and L. A. Taber, 1979; A. A. Parthasarathi et al., 2000) describe the derivation in much greater detail. The model used for our computation is identical to that given in Steele.

Cochlear models show that an increase in orthotropy leads to an increase in the strength of acoustic localization, thus a mem-

Copyright © 2002 by ASME

brane which is much stiffer in the transverse direction than in the longitudinal direction is desired. For this reason we use a beam array rather than a continuous isotropic membrane. (Mid-orthotropic materials such as composites are not readily available at the microscale.) In previous macroscale experimental work (R. D. White and K. Grosh, 2002), it has been demonstrated that WKB models assuming a strongly orthotropic continuous plate model correctly predict the frequency response of a beam array system, although they over-predict the absolute magnitude of the response. Thus, it is admissible to use the continuous model to investigate beam array frequency response.

The cochlear system is driven by a rigid piston, corresponding to the physiological "Stapes", at $x = 0$. This plane wave input produces a traveling wave solution which propagates down the duct, interacting with the membrane, to some location of maximum membrane response. After this location, the wave becomes evanescent, rapidly decaying in amplitude. This has two major advantages. First, it produces a very sharp characteristic cutoff frequency at each location. Secondly, as high frequency components localize at low x, close to the input, they do not propagate down to the wide end of the duct where they could excite higher structural modes.

For a specific example, consider the response of Design 4A-1 (see Table 1) in silicone oil with a density of 962 kg/m^3 and a viscosity of 0.02 $Pa \cdot s$, and taking the mechanical properties of silicon as E=162 GPa, ρ=2330 kg/m^3. Figure 2 gives the frequency response of the center displacement of the beam array at three different locations along the duct ($x = 5mm, 15mm, 25mm$). Response is referenced to pressure at the "Stapes" rigid input piston at $x = 0$. Note the extremely sharp cutoff in the filter characteristics at each location, and also note how the bandwidth of each filter moves as location is changed.

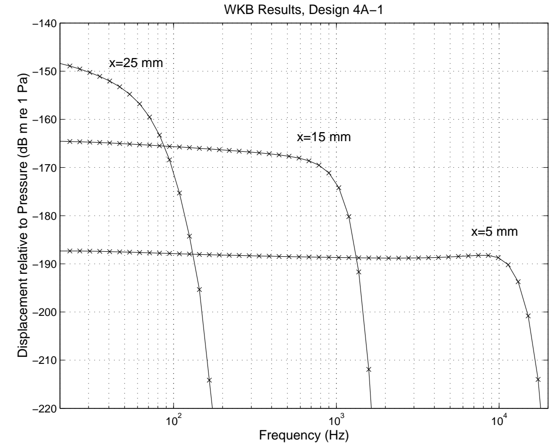

Figure 2. FREQUENCY RESPONSE OF THREE DIFFERENT LOCATIONS ALONG BEAM ARRAY CENTERLINE, REFERENCED TO INPUT PRESSURE AT STAPES, WKB RESULTS FOR DESIGN 4A-1 IN SILICONE OIL

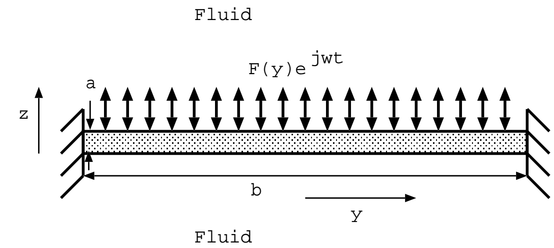

Figure 3. SCHEMATIC OF ISOLATED BEAM MODEL

Isolated Beam Model

An alternative model to the full two-duct WKB model is to treat each beam as an isolated oscillator uncoupled from all other beams in the system. Such a model is more appropriate for the case studied experimentally, where the beam array was excited by a normally incident plane wave in air. This model would not be appropriate for a mid-orthotropic membrane where there is communication through the structure. Nor is it appropriate for use in a fluid system where there is significant communication between adjacent beams through the fluid. However, in the case of a beam-array device operating in air, communication among adjacent beams is minimal. In this situation it is reasonable to consider them as uncoupled and isolated.

The traveling and evanescent wave character predicted for a truly cochlear-like system is lost. This reduces the sharpness of the filter, and also means that higher structural modes can be excited, as all the beams are now exposed to all components of the input waveform.

Following the work by Kirstein et al. (1998) on modeling atomic force microscope (AFM) cantilevers, results are obtained for an isolated clamped-clamped rectangular cross-section beam loaded by an infinite viscous fluid. Equation (2) gives the partial differential equation that arises.

$$\frac{\partial^2 u}{\partial t^2} + \frac{C_s + C_v}{m + m_a}\frac{\partial u}{\partial t} + \frac{EI}{m + m_a}\frac{\partial^4 u}{\partial y^4} = \frac{F(y)e^{j\omega t}}{m + m_a} \quad (2)$$

The fluid has the effect of adding both effective mass and effective damping, reducing the resonant frequency of operation significantly from the in vacuo case. The added fluid mass and damping parameters are

$$m_a = \rho_f w^2 \Re\{H(R_k)\} \quad (3)$$

$$C_v = -\rho_f w^2 \omega \Im\{H(R_k)\} \quad (4)$$

Copyright © 2002 by ASME

where u is membrane displacement in the z direction, $m = \rho w a$ is beam mass per unit length, E is Young's modulus, $I = wa^3/12$ is cross-sectional area moment of inertia, ω is circular excitation frequency, ρ_f is fluid density, C_s is a structural damping parameter, and $F(y,t)$ is force per unit length due to an impinging acoustic wave, harmonic in time with frequency ω. $R_k = \omega w^2/\nu$ is the kinetic Reynolds number (ν is kinematic viscosity), and the complex valued function H is given in equation (5) for an infinite viscous medium. (K_0 and K_1 are the modified Bessel functions of the zeroth and first order, second kind.)

$$H(R_k) = 1 + \frac{4K_1(\sqrt{iR_k})}{\sqrt{iR_k}K_0(\sqrt{iR_k})} \tag{5}$$

Each beam responds as a second order harmonic oscillator at each of its modal frequencies. The results shown can be easily extended to include the shift of natural frequency due to residual tensile or compressive stresses in the beam(R. D. Blevins, 1984). With this extension, the natural frequency and damping factor for each harmonic oscillator is

$$\omega_n = \sqrt{\frac{EI\kappa_n^4}{b^4(m+m_a)}(1+\frac{\sigma_{res}wa}{P_b})}; \tag{6}$$

$$\zeta = \frac{1}{2\omega_n}\frac{Cs+Cv}{m+m_a}; \tag{7}$$

where b is the duct width (And hence the beam length), and σ_{res} is the residual stress. For the clamped-clamped case, $P_b = 4\pi^2 EI/b^2$ is the buckling load, and $\kappa_n = \{4.730..,7.853..,10.996..,14.137..,17.279...\}$ are the structural eigenvalues. When considering the response of each mode, we must select only modal forcing by integrating the spatial function of the impinging force per unit length times the nth mode shape, and then summing over all modes,

$$G(j\omega) = \sum_n \frac{1}{m+m_a}\int_{-b/2}^{b/2}\psi_n(y)\cdot F(y)dy \cdot \frac{1}{(-\omega^2+2\zeta\omega_n j\omega+\omega_n^2)} \tag{8}$$

Note that $F(y)$ is force per unit length, so it is pressure at the interface multiplied by the beam width w. Also note that for a symmetric impinging pressure wave, only symmetric modes will be excited.

The result for Design 4A-1 is given in Figure 4, using 5 modes and for an impinging unit plane wave (i.e. $F(y) = 1$). Residual stress is zero ($\sigma_{res} = 0$). Note that the cutoff is not as sharp as the cochlear model with the incoming traveling wave. The location of the cutoff frequency at each location is similar to the cochlear model.

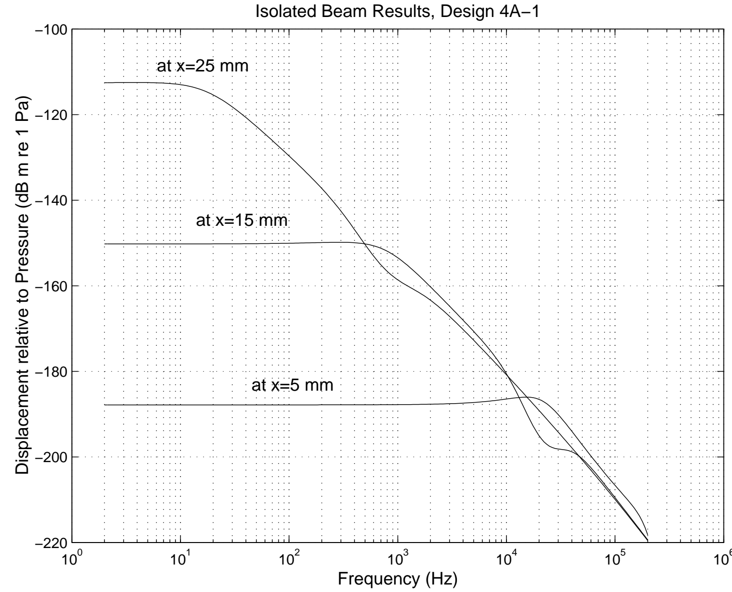

Figure 4. RESPONSE OF BEAM ARRAY CENTERLINE TO IMPINGING UNIT PRESSURE PLANE WAVE, ISOLATED BEAM MODEL RESULTS DESIGN 4A-1 IN SILICONE OIL

Piezoresistive Strain Gauges

In order to sense beam array motion, piezoresistive strain gauges are fabricated by shallow doping of boron into the silicon beams near the built-in ends. The piezoresistive effect causes the resistivity of silicon to shift proportional to the strain evolved in the beam,

$$\rho = \rho_0 \cdot (1 + E\pi_L \varepsilon_{yy}) \tag{9}$$

Where $E\pi_L$ is the longitudinal gauge factor of silicon. The variation of the piezoresistive coefficients for silicon with dopant concentration and crystallographic orientation are discussed in a work by Kanda (1982). Polysilicon piezoresistive properties are discussed by Gridchin et al. (1995) Optimization of dopant profiles and concentrations is discussed fully by Harley and Kenny (2000). In order to balance Johnson noise effects against piezoresistive coefficient, a dopant depth of 1/3 the beam thickness (0.11 μm) and a boron concentration of $1\cdot 10^{19} cm^{-3}$ are desired.

For a clamped-clamped beam in bending, using the Euler-Bernoulli beam model, and assuming a simplification of the modeshape, the strain in the beam is a function of position along the beam, y, and distance from the neutral axis, z,

$$u(\xi) = \delta \sin^2(\frac{\xi\pi}{b}) \tag{10}$$

Copyright © 2002 by ASME

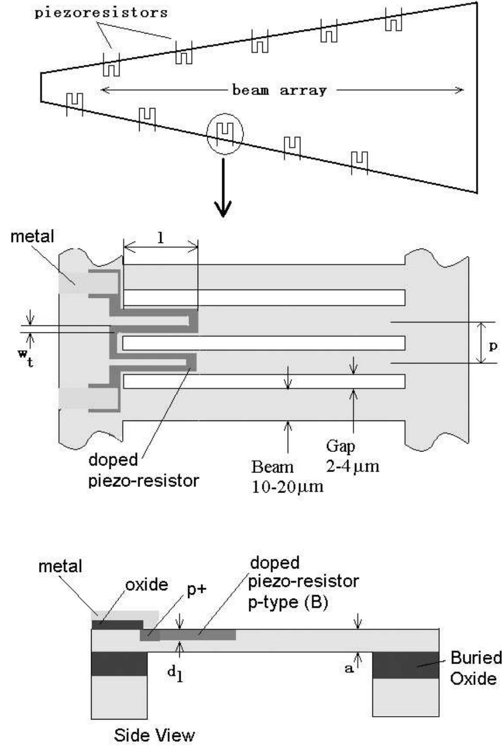

Figure 5. Piezoresistor geometry.

$$\varepsilon_{yy}(\xi,z) = \frac{\partial^2 u}{\partial \xi^2}\cdot z = \delta\frac{\pi^2}{b^2}\cos(\frac{2\xi\pi}{b})\cdot z \tag{11}$$

where $\xi = y - b/2$, b is beam length, and δ is the center displacement of the beam. Computation of the full piezoresistive sensitivity becomes difficult, as the strain is a function of depth and position along the beam, and the dopant profile is a function of depth, which must both be integrated. (Harley, 2000; M. Tortonese, 1993). Instead, following Tortonese, initially assume that the piezoresistive effect is occurring close to the surface, and so use the strain at the surface to compute the unstrained resistance, R, and the resistance change due to bending, ΔR,

$$R = \frac{2\rho_0 l_{leg}}{w_t d_l} \tag{12}$$

$$\Delta R = 2\int_0^{l_{leg}} \frac{\rho_0 E\pi_L \varepsilon_{yy}(\xi, z=a/2)}{w_t d_l} d\xi \tag{13}$$

$$= \delta\frac{\rho_0 E\pi_L \pi a}{b w_t d_l}\sin(2\pi l_{leg}/b) \tag{14}$$

where w_t is the width of the piezoresistor trace, l_{leg} is the length that the trace extends onto the beam, and d_l is the depth of the doped layer. Equations (12) and (14) give the unstrained resistance and change in resistance assuming that the strain is constant at its surface (maximum) value through the thickness of the piezoresistor. It also assumes a sharp constant dopant profile. The errors introduced by these simplifying assumptions can be corrected by use of a parameter β ($0 < \beta < 1$). Then the total fractional resistance change is

$$\frac{\Delta R_{total}}{R_{total}} = \beta\frac{\Delta R}{R} \tag{15}$$

In Harley (2000), the parameter β is given as a function of diffusion length, $\sqrt{Dt}$, and cantilever thickness, a. For our case, $\sqrt{Dt} = 1\cdot 10^{-6} cm$, for boron diffusing at 1000 ^{o}C for 10 secs, and a=0.34μm. Thus, we should use $\beta \approx 0.6$. Also from Harley, we can retrieve a piezoresistive factor for single crystal silicon doped with boron to $1\cdot 10^{19} cm^{-3}$ of $E\pi_L \approx 60$.

In order to maximize sensitivity, $\Delta R_{total}/R_{total}$ must be maximized by appropriate choice of the two remaining design parameters l_{leg} (the length that the piezoresistor extends onto the beam) and N (the number of beams spanned by a single piezoresistor). For our device, the optimal choice of these parameters depends on position down the duct, due to changing beam length and the changing wavenumber of the acoustic response. An optimization procedure has been carried out for the designs in question. The optimal number of beams per piezoresistor varies from 2 to 14, and the optimal length varies from 5% to 15% of the total beam length. (With the smallest length fraction and smallest number of beams per channel at the wide end of the device).

Using the above analysis, the expected sensitivity of the piezoresistive channels, in ppm resistance change per micron of beam center displacement can be computed. For Device 4A-1, channel sensitivity varies logarithmically from 40 ppm/μm for the longest beams to 21,000 $ppm/\mu m$ for the short beams (where strain is higher for a given displacement). However, the shortest beams respond at the highest frequencies, and the longest beams at low frequencies. So, dividing by the modal frequency (in radians/s) of each beam to get response in terms of velocity, we produce an almost constant scale factor of 180 (short beams) - 290 (long beams) $ppm/mm/s$.

Fabrication

Devices have been fabricated out of both single crystal silicon and polysilicon. For the single crystal silicon devices, the starting wafers are 100 mm, 525 μm thick $< 100 >$ SIMOX SOI wafers, with a 3400 Å thick device layer and 4000 Å buried oxide. Both the handle and device layer are initially p-type with a resistivity of 14-22 $\Omega\cdot cm$. The polysilicon devices are fabricated

Copyright © 2002 by ASME

on 500 μm thick $< 100 >$ 100 mm single crystal silicon wafers initially doped p-type to a resistivity of 13 $\Omega \cdot cm$.

Piezoresistor Fabrication

The first stage of the fabrication process defines the electrical portion of the device. The most critical goal of this process is the production of shallow (0.1 μm) junctions for the piezoresistors. The specifics of the fabrication process follow. There are many similarities between this process and that used by Ried, et al to fabricate piezoresistive AFM cantilevers. (1997)

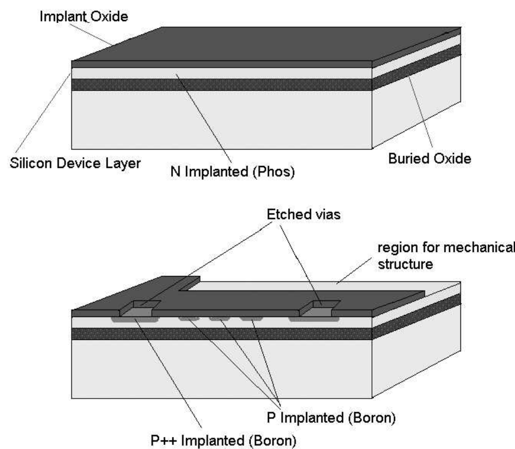

Figure 6. FABRICATION PROCESS FOR PIEZORESISTORS

Process Steps

1. For polysilicon devices, deposit 4000 Å LPCVD oxide at 920 ^oC, 400 mtorr. Deposit 3400 Å LPCVD low stress polysilicon, 588 ^oC, 100 mtorr.
2. For all wafers, deposit 1000 Å LPCVD oxide at 920 ^oC, 400 mtorr.
3. Implant Phosphorus through oxide with dose=$3.4 \cdot 10^{11}$ ions/cm^2, and energy=150 keV to create n-type background for piezoresistor isolation.
4. LPCVD 1000 Å oxide at 920 ^oC, 400 mtorr. Total time at temperature is approximately 1 hr. 30 mins including pumpdown and backfill time. The deposition serves as an anneal for the phosphorus, and also as a thicker passivation and implant oxide.
5. Spin on 1.3 μm thick photoresist, and pattern to expose contact regions. Etch in BHF for 40 secs to thin oxide in contact regions to 1000 Å. This will serve as a feature to align to later on in the process. Implant boron for p++ contacts with dose=$1 \cdot 10^{16}$ ions/cm^2, and energy=40 keV. Strip hardened resist in oxygen plasma.
6. Spin on 1.3 μm thick photoresist, and pattern to expose piezoresistor regions. Implant boron with dose=$4 \cdot 10^{15}$ ions/cm^2, and energy=50 keV. Strip hardened resist in oxygen plasma.
7. Rapid thermal anneal, 12 sec ramp up from room temperature to 1050 ^oC. 10 sec soak at 1050 ^oC. Ramp down to below 400 ^oC in 13 secs. The ramp times are somewhat variable, within a few seconds. This activates the dopants and anneals some of the damage caused by the implant. We desire a shallow junction, so anneal times are short.
8. Spin on 1.3 μm thick photoresist, expose and develop for oxide definition pattern. Etch in BHF for 2.5 mins to open contacts to p++ regions, and clear oxide off the topside of the regions where the mechanical structure will be fabricated.

The piezoresistor fabrication process is very sensitive to both the thickness of the implant oxide deposited in step 4, and the length and temperature of the rapid thermal anneal. TSUPREM4 process simulation software available from Avant! was used to simulate the piezoresistor fabrication process with three different thicknesses of implant oxide. For 100 nm, 150 nm, and 200 nm thick oxides, sheet resistance is 290 Ω/sq, 560 Ω/sq, and 4500 Ω/sq respectively. The sensitivity of sheet resistance to process parameters is indicative of the careful control that is required in order to fabricate functioning piezoresistors. Similar large shifts can be seen if the rapid thermal anneal is not well controlled.

Mechanical Structure Fabrication

Once the piezoresistors have been fabricated, the mechanical structure must be produced. The details and challenges associated with fabrication of the mechanical process are discussed fully in another work (R. D. White and K. Grosh, 2002). In brief, fabrication proceeds by etching the beam pattern using RIE, then sputtering on 500 Å of Cr, followed by 3000 Å of Au. This is patterned by liftoff. Polyimide is then spun on, photodefined, and used to adhesively bond to an oxidized silicon wafer. Deep reactive ion etching (DRIE) is then used to etch through from either side, stopping on the oxide, to define the ducts. Final device release occurs in 1:1 DI:HF etch. See Figure 7.

Etching of the beam structure is successful, as is the metalization step. The Cr/Au has good adhesion to the oxide. A scanning electron microscope picture of the etched beams, boron doped piezoresistor region, and Cr/Au metal line making contact to the piezoresistor is given in Figure 8.

Dicing the wafers after release of the beams is challenging. Coolant water can leak into the structure, despite attempts to seal and protect the beam array, and cause damage. The polyimide wafer bond sometimes fails due to shear during dicing, removing the upper wafer and upper duct. In future design iterations dice lines will be incorporated into the rear duct DRIE mask. The final through-wafer etch will separate the dies, leaving them attached

Copyright © 2002 by ASME

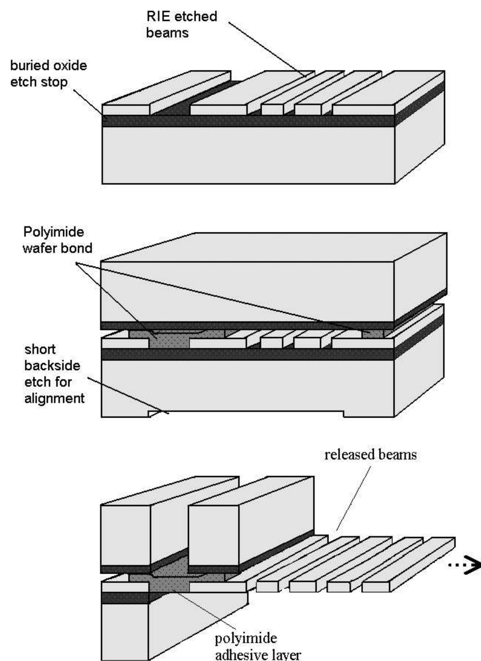

Figure 7. FABRICATION PROCESS FOR MECHANICAL STRUCTURE

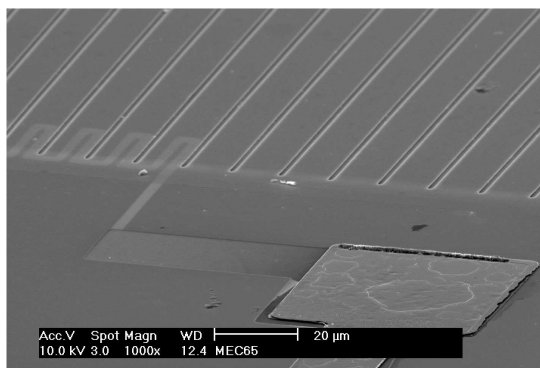

Figure 8. SEM PICTURE OF BEAMS, PIEZORESISTOR, AND METALIZATION FABRICATED ON AN SOI WAFER

to the handle wafer with resist. This will greatly simplify final packaging steps.

Sealing of the duct structures by epoxying on Pyrex covers was unsuccessfully attempted. Silicone oil leaks through the epoxy bond, and there are problems with air bubbles. It will be necessary to redesign the fluidic interface in order to accomplish this feature of the design successfully.

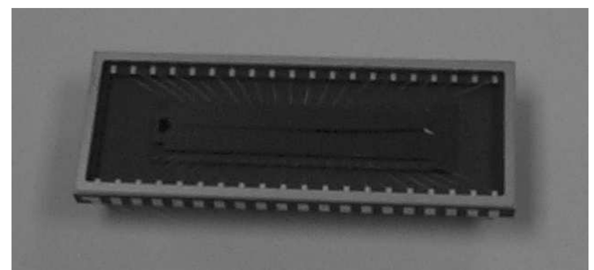

Figure 9. PHOTOGRAPH OF A PACKAGED DEVICE IN THE 40 PIN CDIP PACKAGE, WITH WIREBONDS

Packaging in the 40 pin hybrid ceramic dual inline package (CDIP) package and wirebonding is successful. A photograph of a packaged device is shown in Figure 9. It may be possible to fill the package itself with silicone oil and seal it, rather than continuing with the difficult epoxy/Pyrex process on the wafer.

Piezoresistor Characterization

In order to achieve high sensitivity from the piezoresistors, it is important to keep the dopant close to the wafer surface. Dopant profiles were measured by spreading resistance analysis (SRA) at Solecon Laboratories. Resistivity as a function of depth is determined by beveling the surface at a shallow angle and measuring the spreading resistance at various locations down that beveled incline. From the resistivity data, dopant concentration can be extrapolated.

Due to the cost of SOI wafers, a single-crystal silicon test wafer was used for dopant profiling in single crystal. One of the polysilicon device wafers was used for profiling the polysilicon devices. It is very important to note that the resistivity of polysilicon is much higher than that of single crystal silicon, particularly at low doping levels. At $1 \cdot 10^{18} cm^{-3}$, the resistivity of polysilicon is two orders of magnitude higher than single crystal silicon. From data taken from Ghannam (1988) and Gridchin (1995), an estimated dependence of dopant concentration on resistivity is made. This dependence is used to interpret the SRA results for the polysilicon devices.

The SRA results for the single crystal silicon wafer are given in Figure 10, the results for the polysilicon wafer in Figure 11. The Avant! TSUPREM 4 model very accurately captures the dopant profile in the single crystal test wafer. However, the dopant profile in the polysilicon device has diffused more rapidly than in the single crystal silicon, producing a flat profile. This will greatly reduce the sensitivity of the polysilicon devices. The dopant profile for the p++ highly doped contact region is also given in the figure.

The static resistance values are of interest for comparison with the measured dopant profiles, and are also important for

Copyright © 2002 by ASME

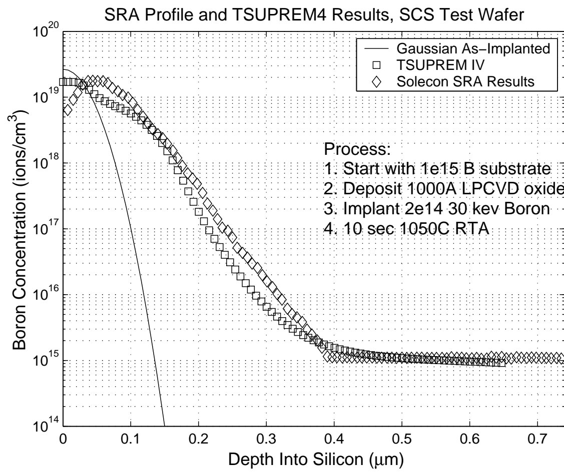

Figure 10. SRA PROFILE WITH MODELS FOR SINGLE-CRYSTAL SILICON TEST WAFER

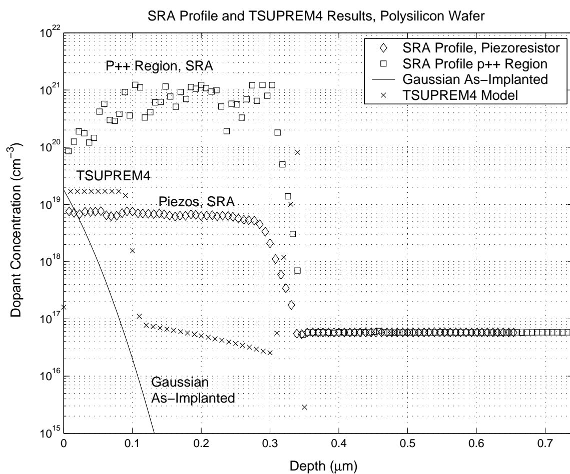

Figure 11. SRA PROFILE WITH MODELS FOR POLYSILICON WAFER

final sensor applications. Table 2 gives a summary of static resistance measurements. Results for probestation measurements of net static resistance are given in the first row. Sheet resistance estimates are made from these static resistance measurements using the known planar geometry of the resistors. These computed sheet resistances are given in the second row. The remaining rows give 4-point probe sheet resistance measurements, and sheet resistance measurements computed by integrating either SRA profiles or TSUPREM4 simulations as noted. The large range given for the SOI wafer TSUPREM4 sheet resistance is due to the previously discussed uncertainty introduced by such process parameters as the implant oxide thickness.

Piezoresistor noise measurements have also been conducted at the wafer level prior to device release using a probe station. Measurements indicate a noisefloor which is consistent with that measured for discrete carbon film resistors of the same value as the piezoresistor channels, for both single crystal and polysilicon devices. 1/f noise characteristics dominate at frequencies below 5 kHz. At high frequencies, the noise floor approaches the expected Johnson noise limit. For a 100 $k\Omega$ resistor (SOI devices are in this range) at room temperature, the Johnson noise floor, $V_{rms}^2 = 4kTR\Delta f$, is approximately 40 $nV/\sqrt{Hz}$.

	SOI	SCS Test	Polysilicon
Net Resistance	50-90 kΩ		400-800 kΩ
Derived Sheet (Ω/sq)	300-350		2900
4-pt. Probe (Ω/sq)		160	2500-3700
SRA Profile (Ω/sq)		480-530	3700
TSUPREM4 (Ω/sq)	290-4500	520	2500

Table 2. STATIC RESISTANCE AND SHEET RESISTANCE MEASUREMENTS

Mechanical Characterization

Mechanical characterization of the MEMS structure has been carried out using a laser Doppler velocimetry (LDV) system. This system measures the velocity of a point from the Doppler shift in the reflected laser light. Our system is a Polytec OFV-303 sensor head, utilizing a class II He-Ne laser with a 633 nm wavelength and a 10 μm minimum spot size. For our purposes, this is coupled with a computer controlled two dimensional micropositioning stage from Newport Corporation. The automated stage is actuated by a VM25.4CCE rolled leadscrew servo motor with 25.4 mm full range of travel, 6 μm on-axis accuracy, and 0.05 μm encoder resolution. There are manual micrometers for course adjustment, allowing an additional 50 mm of travel in each dimension. Computer control of the system is accomplished using Labview software. A National Instruments PCI-6110 data acquisition board with 4 12-bit, 5 MS/s analog inputs, together with a BNC-2110 breakout box, is used for data collection. A Larson-Davis 2520 0.25 inch (6.4 mm) diameter microphone with a 4 Hz to 100 kHz 3dB bandwidth is used for reference. A schematic of the experimental setup is shown in Figure 12.

Mechanical measurements have been conducted in air. Difficulties with intended fluidic packaging have precluded testing in silicone oil. The resonant frequencies of the device shift from the as-designed audio band to ultrasonic frequencies due to the loss of the mass-loading characteristics of a heavy fluid. This poses challenges for testing, as it is more difficult to deliver a well-

Copyright © 2002 by ASME

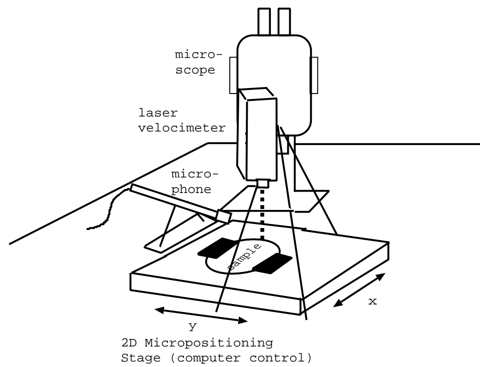

Figure 12. EXPERIMENTAL SETUP FOR LDV MEASUREMENT OF MECHANICAL RESPONSE

characterized excitation at ultrasonic frequencies where wavelengths are short, and where acoustic propagation is highly directional. The best results were obtained by looking at device response to ambient environmental noise, which is non-directional and uncorrelated. Figure 13 gives the power spectrum of four different locations (x=16 *mm*, 20 *mm*, 24 *mm*, 28 *mm*) along the centerline of the device. Results are reported in dB, referenced to spectral content of the acoustic ambient, as measured with the Larson-Davis microphone. The particular curves shown in the figure are for device 4B-4 on an undiced SOI wafer. This device was fabricated for mechanical testing only, and did not go through the piezoresistor fabrication process.

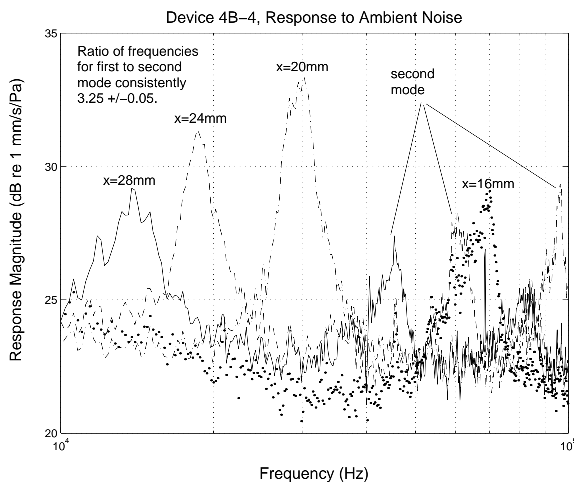

Figure 13. EXPERIMENTAL RESULTS SHOWING RESPONSE OF FOUR LOCATIONS ALONG THE CENTERLINE OF SOI DEVICE 4B-4 OPERATING IN AIR

These devices are operating in air with acoustic excitation impinging normal to the surface. As discussed previously, it is therefore more appropriate to use the isolated beam model for comparison. Comparison of the measured beam resonant frequency along the duct with this model (see equation (7)) is shown in Figure 14. Mechanical properties of air were taken to be $\nu = 15.2 \cdot 10^{-6}\ m^2/s$, $\rho_f = 1.2 kg/m^3$. Mechanical properties of silicon were taken to be E=162 GPa, ρ=2330 kg/m^3. The geometry was as described in Table 1, with beam thickness of 0.32 μm. (Measured film thickness)

Response of the second mode of beam oscillation can also be seen in Figure 13. The ratio between the first and second modal frequencies determined experimentally is 3.3. For a clamped-clamped beam, the predicted ratio is 2.8.

Adding 1.3 *MPa* of tensile residual stress into the model improves agreement between predicted and measured resonant frequencies. Any remaining discrepancies between the predicted and measured resonant frequencies could be due to variation in residual stress with position. It seems likely that there are small variations in residual stress with position, since a small tensile residual stress is used to shift the model into agreement with experiment, yet many beams longer than 500 μm buckle, indicating a small compressive residual stress in some regions.

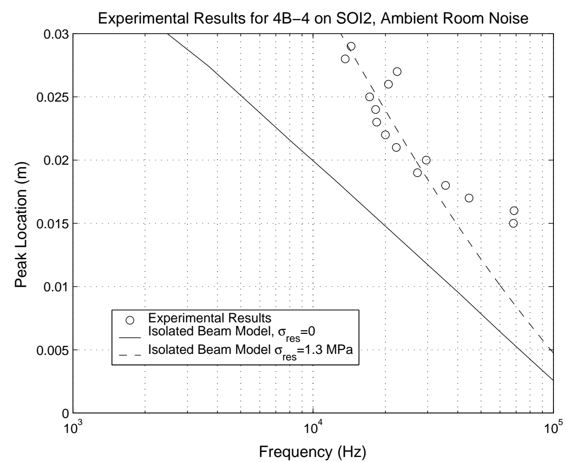

Figure 14. COMPARISON OF EXPERIMENTALLY DETERMINED RESONANT FREQUENCY AS A FUNCTION OF X WITH ISOLATED BEAM MODEL FOR 0 AND 1.3 MPA OF TENSILE RESIDUAL STRESS

The amplitude of the response is also in reasonable agreement with the isolated beam model. The model predicts 35-40 dB re 1 $mm/s/Pa$. Experiment indicates approximately 28-33 dB re 1 $mm/s/Pa$.

 Copyright © 2002 by ASME

Conclusions

Device modeling demonstrates that a cochlear-like system with fluid loaded beams and a duct system enforcing an incoming traveling wave produces mechanical filtering with very sharp cutoff. The filtration characteristics are significantly better than that accomplished by an array of isolated, uncoupled beams excited by normally incident acoustic radiation.

Piezoresistor modeling has allowed optimal choice of piezoresistor geometry at each location along the length of the transducer. The expected sensitivity for device 4A-1 varies logarithmically from 40 ppm resistance change per μm of center displacement for the longest beams to 21,000 $ppm/\mu m$ for the shortest beams. For response at their resonant frequency, this translates to 180 (short beams) - 290 (long beams) ppm resistance change per mm/s of center velocity.

Fabrication of the piezoresistors and the suspended mechanical structure in air have been completed successfully. Device sealing and fluidics has proved difficult and has not yet been accomplished. Buckling of beams longer than 500 μm occurs, and there are issues of stiction for the longest beams. Dicing operations are difficult with the fragile structure released, thus it is advisable to design the process in such a way as to avoid mechanical dicing after release.

Dopant profiles indicate that TSUPREM4 simulations were very accurate in predicting dopant profiles produced in single crystal silicon by ion implantation and subsequent rapid thermal annealing. However, the profiles are very sensitive to process parameters such as implant oxide thickness and anneal time. Also, boron diffusion in polysilicon was observed to be much more rapid than in single crystal silicon, creating a flat profile which will not be sensitive to bending strain.

Mechanical measurements of structure mechanical response in air, conducted with a laser Doppler velocimetry system, demonstrate good modeling of device resonant frequencies using the isolated beam model. 1.3 MPa of tensile residual stress improves agreement between the model and experiment. Response magnitude is 28-33 dB relative to 1 $mm/s/Pa$, which is close to that predicted by the isolated beam model with a normally incident plane wave. (35-40 dB re 1 $mm/s/Pa$ predicted)

The experimentally and theoretically determined response magnitude, in conjunction with the predicted piezoresistor sensitivity, suggests that device sensitivity in air will be 7000 ppm resistance change per Pascal of incident acoustic pressure. With 10 Volts of excitation to a Wheatstone bridge, and the Johnson noisefloor of a 100 $k\Omega$ resistor of approximately 40 $nV/\sqrt{Hz}$ at room temperature, this translates to a predicted device resolution of 250 μPa_{rms} acoustic pressure in a 100 kHz band in air.

Future work will continue to characterize device response. Additional measurements will be made in air, including harmonic excitation of structural response and an examination of structural modeshape. Fluid loaded devices will also be tested in silicone oil and compared with models. Piezoresistor test circuits will be constructed and used to measure the frequency response of each piezoresistive channel.

A second design iteration will utilize low-stress nitride beams with deposited polysilicon strain gauges. This will address the issue of buckling due to film residual stress, as residual stresses produced during nitride deposition will be tensile. In addition, the polysilicon piezoresistors can be uniformly doped due to the layered structure, removing the stringent requirements on the implantation and annealing process.

REFERENCES

R. D. Blevins. *Formulas for Natural Frequency and Mode Shape*. R. E. Krieger, Malabar, Fla., 1984.

M.Y. Ghannam and R.W. Dutton. Resistivity of boron-doped polycrystalline silicon. *Applied Physics Letters*, 52:1222–1224, 1988.

Graff, K. (1975). *Waves in Elastic Solids*. Ohio State Univ. Press, Cols., OH.

V.A. Gridchin, V.M. Lubimsky, and M.P. Sarina. Piezoresistive properties of polysilicon films. *Sensors and Actuators A*, 49: 67–72, 1995.

J. Harley and T. Kenny. 1/f noise considerations for the design and process optimization of piezoresistive cantilevers. *Journal of Microelectromechanical Systems*, 9:226–235, 2000.

J. A. Harley. *Advances in Piezoresistive Probes for Atomic Force Microscopy*. PhD thesis, Stanford University, 2000.

Y. Kanda. A graphical representation of the piezoresistance coefficients in silicon. *IEEE Transactions on Electronic Devices*, 29, 1982.

S. Kirstein, M. Mertesdorf, and M. Schonhoff. The influence of a viscous fluid on the vibration dynamics of scanning near-field optical microscopy fiber probes and atomic force microscopy cantilevers. *Journal of Applied Physics*, 84, 1998.

J.T. Oden and E.A. Ripperger (1981). *Mechanics of Elastic Structures*. Hemisphere Publishing, Washington, DC, second edition.

A. A. Parthasarathi, K. Grosh, and A. L. Nuttall. Three-dimensional numerical modeling for global cochlear dynamics. *J. Acoust. Soc. Amer.*, 107:474–485, 2000.

R. P. Ried and L. S. Fan. 6-mhz 2-n/m piezoresistive atomic-force-microscope cantilevers with incisive tips. *Journal of Microelectromechanical Systems*, 6:294–302, 1997.

C. R. Steele and L. A. Taber. Comparison of wkb calculations and experimental results for three-dimensional cochlear models. *J. Acoust. Soc. Amer.*, 65:1007–1018, 1979.

M. Tortonese. *Force Sensors for Scanning Probe Microscope*. PhD thesis, Stanford University, 1993.

R. D. White and K. Grosh. A micromachined cochlear-like acoustic sensor. In *Proceedings of the SPIE*, volume 4700, 2002.

Copyright © 2002 by ASME